



**HAL**  
open science

# Supramolecular synthon pattern in solid clioquinol and cloxiquine (APIs of antibacterial, antifungal, antiaging and antituberculosis drugs) studied by CI NQR, H-O and H-N NQDR and DFT/QTAIM

Jolanta Natalia Latosińska, Magdalena Latosińska, Marzena Agnieszka Tomczak, Janez Seliger, Veselko Žagar

## ► To cite this version:

Jolanta Natalia Latosińska, Magdalena Latosińska, Marzena Agnieszka Tomczak, Janez Seliger, Veselko Žagar. Supramolecular synthon pattern in solid clioquinol and cloxiquine (APIs of antibacterial, antifungal, antiaging and antituberculosis drugs) studied by CI NQR, H-O and H-N NQDR and DFT/QTAIM. *Journal of Molecular Modeling*, 2010, 17 (7), pp.1781-1800. 10.1007/s00894-010-0876-4. hal-00642398

**HAL Id: hal-00642398**

**<https://hal.science/hal-00642398>**

Submitted on 18 Nov 2011

**HAL** is a multi-disciplinary open access archive for the deposit and dissemination of scientific research documents, whether they are published or not. The documents may come from teaching and research institutions in France or abroad, or from public or private research centers.

L'archive ouverte pluridisciplinaire **HAL**, est destinée au dépôt et à la diffusion de documents scientifiques de niveau recherche, publiés ou non, émanant des établissements d'enseignement et de recherche français ou étrangers, des laboratoires publics ou privés.

# Supramolecular synthon pattern in solid clioquinol and cloxiquine (API of antibacterial, antifungal, antiaging and antituberculosis drugs) studied by $^{35}\text{Cl}$ NQR, $^1\text{H}$ - $^{17}\text{O}$ and $^1\text{H}$ - $^{14}\text{N}$ NQDR and DFT/QTAIM

Received: 18.04.2010 / Accepted: 14.09.2010

Jolanta N. Latosińska<sup>1,✉</sup>, Magdalena Latosińska<sup>1</sup>, Marzena A. Tomczak<sup>1</sup>, Janez Seliger<sup>2,3</sup>, and Veselko Žagar<sup>2</sup>

<sup>1</sup>Faculty of Physics, Adam Mickiewicz University, Umultowska 85, 61-614 Poznań, Poland

<sup>2</sup>“Jozef Stefan” Institute, Jamova 39, 1000 Ljubljana, Slovenia

<sup>3</sup> Faculty of Mathematics and Physics, University of Ljubljana, Jadranska 19, 1000 Ljubljana, Slovenia

✉Tel.: +48-61-8295277; Fax: +48-61-8257758; E-mail: Jolanta.Latosinska@amu.edu.pl

## Abstract

Quinolinol derivatives: clioquinol (5-Chloro-7-iodo-8-quinolinol, Quinoform) and cloxiquine (5-Chloro-8-quinolinol) have been studied experimentally in solid state by the  $^{35}\text{Cl}$  NQR,  $^1\text{H}$ - $^{17}\text{O}$  and  $^1\text{H}$ - $^{14}\text{N}$  NQDR spectroscopies and theoretically by the *Density Functional Theory* (DFT). The supramolecular synthon pattern: O-H...N hydrogen bonds linking dimers as well as stacking  $\pi$ - $\pi$  interaction have been described within the QTAIM (*Quantum Theory of Atoms in Molecules*) /DFT (*Density Functional Theory*) formalism. Both proton donor and acceptor sites in O-H...N bonds were characterized using the  $^1\text{H}$ - $^{17}\text{O}$  and  $^1\text{H}$ - $^{14}\text{N}$  NQDR spectroscopies and QTAIM. The possibility of existence of O-H...H-O dihydrogen bonds was excluded. The weak intermolecular interactions in the crystals of clioquinol and cloxiquine were detected and examined. The results obtained in this work suggest that considerable differences in the NQR parameters for the planar and twisted supramolecular synthons permit differentiation between specific polymorphic forms and indicate that the higher planarity of supramolecular synthons is

accompanied with a greater number of weaker hydrogen bonds linking them and stronger  $\pi\cdots\pi$  stacking interaction.

**Keywords** Clioquinol, cloxiquine · Nuclear Quadrupole Resonance · Anti-aging · Anti-cancer · Anti-tuberculosis · Anti-bacterial · Anti-fungal · DFT · QTAIM · Intermolecular interactions · Supramolecular synthon · Polymorphism

## Introduction

Quinolinol derivatives: clioquinol (5-Chloro-7-iodo-8-quinolinol, Quinoform; Quinambicide; Vioform) and cloxiquine (5-Chloro-8-quinolinol, Chloroxychinolin, Cloxiquine, Dermofongin A) Fig. 1 are active pharmaceutical ingredients (API) of a wide spectrum of known potent antibacterial, antifungal and antiamebic agents used in the treatment of dermatoses [1-3] and antiseptic or disinfectant formulations [4] known for decades. Both are members of the group of drugs called 8-quinolinols which inhibit DNA replication and are active against both viral and protozoal infections [5]. Clioquinol is also used to treat diarrhoea and other gastrointestinal disorders, skin infections such as eczema, athlete's foot, jock itch, ringworm and active against some bacteria: *Staphylococccen*, *Streptococccen*, *E. coli*, yeasts *Candida albicans*, and some protozoal parasites, particularly *Trichomonas sp.* [6, 7] and recently tuberculosis [8]. On the other hand, both clioquinol and cloxiquine are common causes of epigastric discomfort, contact dermatitis and neuropathy and both are considered as mutagens. Clioquinol produces not only allergic reactions, eosinophilia or hyperthyreosis but also having teratogenic and carcinogenic effects is the most toxic among the antibacterial compounds which can depress the central nervous system and was out of internal use in the 1970s due to serious adverse events like: blindness, paralysis or death [9]. The increasing interest in both compounds stems from the recent finding that cloxiquine has been recently reported to exhibit good antituberculosis activity even for multidrug resistant (MDR) isolates [10], whereas clioquinol, which is known to be extremely neurotoxic (on account of its ability to chelating metals [11]) in large doses and is one of the agents leading to the lethal subacute myelo-optico-neuropathy (SMON) [12, 13], in small doses has been found capable of reversing the progression of neurodegenerative disorders. The latter effect is probably due to the action directed directly to the protein called CLK-1 ("clock-1") and thus helpful against Alzheimer's, Parkinson's and Huntington's diseases by slowing aging [14-17], which is connected with free radical scavenging capabilities. Very recently, Clioquinol has been found to inhibit proteasome, display preclinical activity in leukemia and myeloma [18] and to have anticancer effects both *in vitro* and *in vivo* [19]. Unfortunately, the mechanism of its action has not been even located yet, although, it is supposed to be related with the iodine content.

In regard of the above, comparison of the structural and electronic properties of clioquinol and cloxiquine (differing from clioquinol only by the lack of iodine at 7 position of the quinoline ring), seems very promising from the point of view of differences in their biological activity, and

therefore deserves detailed studies. It is known that biological activity of compounds is related to their chemical structure, especially electron density distribution and bonding capabilities [20, 21]. Since the first experiments in solid-state Nuclear Quadrupole Resonance (NQR), a great potential of this molecular specific method, offering a possibility of non-destructive characterization of solid pharmaceutical products, in the analysis of biological systems has been recognized [22-25]. The electric field gradient (EFG) tensor depends on the position and charge of the nuclei and electrons about the quadrupolar nucleus and thus the quadrupole coupling constant, which is the greatest in magnitude principal value of the EFG tensor multiplied by the nuclear quadrupole moment and divided by the Planck's constant, reflects the electron distribution in the vicinity of the quadrupolar nuclei, and thus it is a very sensitive tool for investigation of details of the molecular and crystal structure. To study clioquinol and cloxiquine NQR seems to be the optimal method of choice, because both compounds contain, which is really rare, three kinds of quadrupolar nuclei in a molecule:  $^{14}\text{N}$ ,  $^{17}\text{O}$  and  $^{35}\text{Cl}$  (for clioquinol even four including  $^{127}\text{I}$ ). In order to elucidate these details and to contribute to the understanding of the differences in biological activity of both compounds, we performed a joint study using NQR on different isotopes  $^{14}\text{N}$ ,  $^{17}\text{O}$  and  $^{35}\text{Cl}$  atoms and the Density Functional Theory (DFT) which reveals local and global, electron distribution density in the molecule. We expect that this combined study will facilitate the detail understanding of the differences in structural features of clioquinol and cloxiquine, and contribute to the explanation of the role of clioquinol on the molecular level, especially the functional implications of iodine substitution and O-H...N hydrogen bonding formation for recognition and binding of clioquinol molecules to the mitochondrial enzyme CLK-1 (also known as COQ7).

## Experimental

High purity polycrystalline samples of clioquinol and cloxiquine (95% and 97%, respectively) were purchased from Sigma-Aldrich and used without any additional purification.

### NQR spectroscopy

The  $^{35}\text{Cl}$ ,  $^{17}\text{O}$  and  $^{14}\text{N}$  nuclei have spin  $I=3/2$ ,  $5/2$  and  $1$ , respectively and therefore in zero magnetic field  $^{35}\text{Cl}$  exhibits two,  $^{17}\text{O}$  exhibits three doubly degenerated while  $^{14}\text{N}$  exhibits nondegenerated nuclear quadrupole energy levels. Their energies depend on the nuclear

quadrupole moment  $eQ$  and on the electric-field-gradient (EFG) tensor  $V_{ik} = \partial^2 V / \partial x_i \partial x_k$ , composed of the second derivatives of the electrostatic potential  $V$  with respect to the coordinates at the position of the nucleus. The symmetric traceless second rank EFG tensor has three principal values:  $V_{ZZ} = eq$ ,  $V_{YY}$  and  $V_{XX}$  ( $|V_{ZZ}| > |V_{YY}| \geq |V_{XX}|$ ) which are used to obtain two unique NQR parameters: the nuclear quadrupole coupling constant ( $e^2Qq/h$ ) and asymmetry parameter ( $\eta$ ), interrelated with the NQR frequencies ( $\nu$ ) through the following equations [26].

a) For  $^{35}\text{Cl}$  the frequencies do not uniquely depend on the quadrupole coupling constant  $e^2qQ/h$  and the asymmetry parameter  $\eta$ :

$$\nu(^{35}\text{Cl}) = \frac{e^2Qq}{2h} \sqrt{1 + \eta^2/3} \quad (1)$$

but for biologically active compounds the values of  $\eta \ll 0.1$ .

b) For  $^{17}\text{O}$ , the three NQR frequencies usually named as  $\nu_{5/2-1/2} > \nu_{5/2-3/2} \geq \nu_{3/2-1/2}$ , uniquely depend on  $e^2qQ/h$  and  $\eta$ , but can be calculated with the use of the following secular equation:

$$x^3 - 7(3 + \eta^2)x - 20(1 - \eta^2) = 0. \quad (2)$$

where  $x$  is a solution of (2) and the energies of the NQR levels can be calculated using the formula  $E = (e^2qQh^{-1}/20)x$ .

c) For  $^{14}\text{N}$  the three NQR frequencies similarly to those for  $^{17}\text{O}$ , usually named as  $\nu_+ > \nu_- \geq \nu_0$  uniquely depend on the quadrupole coupling constant  $e^2qQ/h$  and the asymmetry parameter  $\eta$ :

$$\begin{aligned} \nu_+(^{14}\text{N}) &= \frac{e^2Qq}{4h} (3 + \eta) \\ \nu_-(^{14}\text{N}) &= \frac{e^2Qq}{4h} (3 - \eta) \\ \nu_0(^{14}\text{N}) &= \nu_+(^{14}\text{N}) - \nu_-(^{14}\text{N}) = \frac{e^2Qq}{2h} \eta \end{aligned} \quad (3)$$

The natural abundance of the  $^{35}\text{Cl}$  isotope is high (75.4 %) and the NQR frequencies are typically between 30-40 MHz so it is possible to use pure NQR experimental technique. The natural

abundance of the  $^{14}\text{N}$  isotope is very high (99.636 %) but the NQR signals are weak and in addition the NQR frequencies are typically between 0.5-4 MHz thus the use of  $^1\text{H}$ - $^{14}\text{N}$  NQDR technique is preferred than the use of pure NQR. The natural abundance of the  $^{17}\text{O}$  isotope is rather low (0.037 %) and the NQR frequencies are typically below 5 MHz thus the use of several  $^1\text{H}$ - $^{17}\text{O}$  NQDR techniques is required.

### **$^1\text{H}$ - $^{14}\text{N}$ -NQDR**

Different double resonance techniques based on magnetic field cycling were used to detect  $^{14}\text{N}$  NQR frequencies. The proton spin system was polarized in  $B_0 = 0.75$  T for 30 seconds. Then the sample was within 0.1 s pneumatically transferred into another magnet where it was left for 0.3 s. In this other magnet the magnetic field can be varied continuously between zero and 0.1 T. After the stay in this other magnet the sample was within 0.1 s pneumatically transferred back into the first magnet and the proton NMR signal was measured immediately after the sample had been stopped in the first magnet.

As the first method we used the  $^1\text{H}$ - $^{14}\text{N}$  cross relaxation spectroscopy [27-29]. In this method the sample is left to relax in a low magnetic field for a fixed time  $\tau$  (in our case  $\tau = 0.5$  s) and the low magnetic field is varied between the magnetic field cycles in steps of approximately 0.5 mT corresponding to the step in the proton Larmor frequency  $\nu_L$  of 20 kHz. The proton Larmor frequency range between 0 kHz and 4 MHz is usually scanned by this technique. When the proton Larmor frequency  $\nu_L$  matches a  $^{14}\text{N}$  NQR frequency  $\nu_Q$  the proton spin-lattice relaxation time shortens, which results in a decrease in the proton NMR signal after the cycle. In some cases, especially at higher proton Larmor frequencies, the step of 40 kHz can be used. On the other hand, around  $\nu_L = \nu_Q$  the step is reduced to 10 kHz to improve the resolution.

In the second step we used the solid-effect technique [30]. In this method the low magnetic field was fixed at a value  $B$ , corresponding to the proton Larmor frequency  $\nu_L = \gamma_{\text{H}}B/2\pi$ , and the sample was in the low magnetic field irradiated for 0.5s with a strong rf magnetic field at variable frequencies. When the frequency  $\nu$  of the rf magnetic field is equal to  $\nu = \nu_Q \pm \nu_L$ , simultaneous spin flips take place in both  $^1\text{H}$  and  $^{14}\text{N}$  spin systems and, as a result, the proton magnetization drops to a lower value. The experiment is repeated at a few values of the low magnetic field to clarify the spectrum and to get rid of the signal artefacts caused by the direct

proton absorption of the rf power at multiples of the proton Larmor frequency and the level crossing signals produced by the higher harmonics of the rf magnetic field.

As the final technique, combining the three  $^{14}\text{N}$  NQR frequencies from a given nitrogen site, we used the two-frequency irradiation technique [31]. Here the proton Larmor frequency  $\nu_L$  in the low magnetic field is set in resonance with the lowest  $^{14}\text{N}$  NQR frequency  $\nu_0$  and the sample is irradiated with two rf magnetic fields at the frequencies  $\nu_1 = \nu$  and  $\nu_2 = \nu + \nu_0$ . When  $\nu_1 = \nu_-$  and  $\nu_2 = \nu_- + \nu_0 = \nu_+$ , the proton relaxation rate in the low magnetic field increases and, as a result, the proton NMR signal at the end of the magnetic field cycle drops to a low value. This technique is applied to solve complex  $^{14}\text{N}$  NQR spectra to help separate between triplets corresponding to various nitrogen positions in the crystal.

### **$^1\text{H}$ - $^{17}\text{O}$ NQDR**

The  $^{17}\text{O}$  NQR frequencies in 5-chloroquinol have been first measured by the Slusher and Hahn' technique [32]. The sample was pneumatically moved between two magnets with the magnetic field  $B_0 = 0.75$  T and zero. The proton spin system was in the high magnetic field  $B_0$  polarized for 30 second and then transferred into zero magnetic field for 0.8 s. Then the sample was transferred back into the first magnet and the intensity of the proton NMR signal was measured immediately after the sample stopped in the high magnetic field. The sample was in zero static magnetic field, irradiated with a phase-modulated rf magnetic field with the frequency  $\nu$  and with the amplitude about 3 mT. A square wave  $180^\circ$  phase modulation was used with the frequency 1.7 kHz. The frequency  $\nu$  was changed between the repetitive magnetic field cycles in steps of 20 kHz. The frequency range between 1.0 MHz and 5.0 MHz was scanned by the frequency  $\nu$ . Two dips corresponding to the  $^{17}\text{O}$  NQR frequencies  $\nu_{3/2-1/2}$  and  $\nu_{5/2-3/2}$  are usually observed by this technique. The third dip at the highest  $^{17}\text{O}$  NQR frequency  $\nu = \nu_{5/2-1/2}$  has, as shown in [33], a much lower intensity than the other two dips and is usually not observed by the Slusher and Hahn's technique.

During the second part of the experiment we used the two-frequency irradiation technique [34] to determine the dipolar structure of the  $^1\text{H}$ - $^{17}\text{O}$  NQDR lines. Two rf magnetic fields of the frequencies  $\nu_1$  and  $\nu_2$  were applied in repetitive pulses at the frequencies  $\nu_1, \nu_2, \nu_1, \nu_2, \dots$ . The duration of a pulse was 1 ms. The amplitude of the rf magnetic field was for the measurement of

the dipolar structure of the NQDR lines at  $\nu = \nu_{3/2-1/2}$  and  $\nu = \nu_{5/2-3/2}$  reduced to 0.3 mT. The dipolar structure of the highest frequency NQDR line was measured with rf magnetic fields with the amplitude of 3 mT., due to the lower transition probability per unit time.

The dipolar structure of a NQDR line was determined in two experiments. The first of the two frequencies, say  $\nu_1$ , was fixed at the lower edge of the NQDR line and the line was scanned at the second frequency  $\nu_2$  in steps of 5 kHz. No drop in the proton NMR signal was observed when  $\nu_1 = \nu_2$ . The strongest drop in the proton NMR signal was observed when  $\nu_2$  was in the upper part of the NQDR line. To determine the dipolar structure of the lower part of the NQDR line, the experiment was repeated with the frequency  $\nu_1$  fixed at the upper edge of the NQDR line. The dipolar structures of the three NQDR lines determined by the two-frequency irradiation was analysed according to [35].

### **<sup>35</sup>Cl-NQR**

The <sup>35</sup>Cl-NQR spectra of clioquinol and cloxiquine were taken at 77 K. The NQR signals assigned to Cl nuclei were weak (S/N=3 after 1000 accumulations) and the resonance line was wide (a full width at half maximum (FWHM) was 27 kHz), therefore, the classical Hahn sequence  $\pi - \tau - 2\pi$  was applied. Because in NQR of a powdered sample both the excitation and the reception of the signal depend on the relative orientation of the crystallites with respect to the coil axis, the pulse sequence was optimized and the optimized pulse length 5  $\mu$ s and the interval between the pulses was 90  $\mu$ s. The NQR lineshape was obtained from the fast Fourier transform (FFT) of the both half-echo signals after 1000 accumulations for the desired signal-to-noise ratio. The repetition time of the scans was 200 ms. The accuracy of the <sup>35</sup>Cl-NQR frequency determination was of about 10 kHz.

### **DFT calculations**

Quantum chemical calculations were carried out within the GAUSSIAN03<sup>TM</sup> code [36] run on the CRAY supercomputer at the Poznan Supercomputer and Network Centre (PCSS) in Poznan, Poland. All calculations were performed within the Density Functional Theory (DFT) with exchange-correlation hybrid functional: B3LYP (three-parameter exchange functional of Becke

B3 [37] combined with the Lee–Yang–Parr correlation functional LYP [38]) using the extended basis sets with polarization and diffuse functions 6-311++G\*\*. The calculations were carried out under the assumption of the crystallographic as well as the partially optimized geometry, where during optimization made using Berny algorithm, only the positions of the hydrogen atoms were allowed to relax while those of all other atoms remained frozen. The NQR parameters: quadrupole coupling constants, asymmetry parameters and frequencies at all nitrogen atoms were calculated assuming different polymorphic forms, which differed in molecular aggregations formed as a result of intermolecular interactions.

Theoretical analysis of the intermolecular interactions was performed within the quantum theory of atoms in molecules theory (QTAIM) [39] and the topological parameters were calculated, including the bond critical points (BCP), ring critical points (RCP), Laplacian of the electron density ( $\Delta\rho$ ) and ellipticity of the bond ( $\epsilon$ ), the total electron energy density at BCP ( $H_{\text{BCP}}$ ) and its components: the local kinetic energy density ( $G_{\text{BCP}}$ ) and the local potential energy density ( $V_{\text{BCP}}$ ). Because of the basis dependence on the atomic position, i.e. basis set superposition error (BSSE), the small interaction energies are often overestimated thus the interaction energies were corrected for BSSE by the standard counterpoise (CP) method [40]. Another correction was made for the zero point vibrational energies (ZPVE). However, this approach is not useful for the intramolecular or multiple hydrogen bonds thus the energy of interactions was calculated according to Espinosa [41].

## Results and discussion

The  $^{35}\text{Cl}$ -NQR spectra of clioquinol and cloxiquine are presented in Fig. 2. We observe only one resonance line at 35.170 MHz for clioquinol and at 34.787 MHz for cloxiquine at 77K. All the molecules are thus crystallographically equivalent in each of the two compounds, which is in agreement with the X-ray data [42-45].

The  $^1\text{H}$ - $^{14}\text{N}$  NQDR spectra of clioquinol and cloxiquine as obtained by the solid-effect technique at  $T = 295$  K are presented in Fig. 3. Seven NQDR lines are unambiguously resolved in each spectrum. However, as shown in [29], the intensities of the NQDR lines differ strongly when the population of the energy levels of the nitrogen spin system approaches the Boltzmann population slower than that of the energy levels of the proton spin system. A triplet is usually observed at

$\nu = \nu_+ - \nu_L$ ,  $\nu_+$  and  $\nu_+ + \nu_L$ . The solid effect lines  $\nu = \nu_0 - \nu_L$  and  $\nu = \nu_- - \nu_L$  are usually missing. Having this in mind and on the basis of the previously recorded cross relaxation spectra, we can determine the  $^{14}\text{N}$  NQR frequencies as 3.330 MHz, 2.830 MHz and 0.500 MHz for cloxiquine and 3.410 MHz, 2.830 MHz and 0.580 MHz for clioquinol. The accuracy is 10-20 kHz. A more precise determination of the  $^{14}\text{N}$  NQR frequencies to the accuracy of  $\pm 2$  kHz was obtained using the two-frequency irradiation technique. The  $^{14}\text{N}$  NQR frequencies: 3.328 MHz, 2.828 MHz and 0.500 MHz for cloxiquine and 3.407 MHz, 2832 MHz and 0.575 MHz for clioquinol, are not far from the frequencies determined from the solid effect spectra. All nitrogen positions are crystallographically equivalent in cloxiquine as well as in clioquinol.

The  $^1\text{H}$ - $^{17}\text{O}$  NQDR spectrum was measured only of cloxiquine. Due to the low natural abundance of  $^{17}\text{O}$  (0.037%) the sensitivity of the NQDR technique strongly depends on the proton spin-lattice relaxation time in zero magnetic field, which should be about 1 second or more to observe the NQDR dips. For cloxiquine we obtained a long enough proton spin-lattice relaxation time in zero magnetic field by reducing the temperature of the sample to 213 K. For clioquinol we also varied the temperature of the sample, but within the working range of the spectrometer (130 K – 400 K) we did not observe long enough proton  $T_1$  in zero magnetic field. This is presumably the effect of the  $^{127}\text{I}$  contribution to the spin-lattice relaxation of the proton dipolar system.

The  $^1\text{H}$ - $^{17}\text{O}$  NQDR spectrum of cloxiquine as obtained by the Slusher and Hahn's technique is presented in Fig. 4a. Two NQDR dips are observed at the frequencies 2.425 and 1.750 MHz. These two dips correspond to the  $^{17}\text{O}$  NQR frequencies  $\nu_{5/2-3/2}$  and  $\nu_{3/2-1/2}$ , respectively. The third dip expected at the frequency  $\nu_{5/2-1/2} = \nu_{5/2-3/2} + \nu_{3/2-1/2} = 4.175$  MHz is too weak to be observed by the Slusher and Hahn's technique.

The dipolar structure of the three  $^{17}\text{O}$  NQR lines, as measured by the two-frequency irradiation technique, is presented in Fig. 4b. Also the 5/2-1/2 transition is observed by this technique. The dipolar structure of the three  $^{17}\text{O}$  NQR lines is not well resolved due to the proton-proton dipolar interaction. Nevertheless it is still possible to determine the proton-oxygen distance plus the polar angle  $\theta$  and the azimuthal angle  $\phi$  describing the orientation of the O-H bond in the principal-axis frame of the EFG tensor at the position of the oxygen nucleus from the widths of the dipolar split  $^{17}\text{O}$  NQR lines [34]. The results are as follows. The O-H distance is  $0.99 \pm 0.01$

Å. The O-H bond lies in the x-z plane of the EFG tensor ( $\varphi = 0^0$ ) and makes an angle  $\theta = 50^0 \pm 5^0$  with the principal axis z of the EFG tensor.

The experimental  $^{14}\text{N}$ ,  $^{17}\text{O}$  and  $^{35}\text{Cl}$  NQR frequencies and those calculated on the basis of them  $e^2Qqh^{-1}$  and  $\eta$  for both compounds are collected in Table 1. As follows from these results, all the clioquinol as well as cloxiquine molecules in the elementary cell are equivalent within the experimental resolution, which is in a good agreement with the X-Ray data according to which clioquinol crystallizes in the monoclinic system P2/c or P2/a [42, 43], while cloxiquine crystallizes in the orthorhombic system Fdd2 (form I) or the monoclinic system P2/c (form II) [44, 45].

Parameters of the elementary cells of cloxiquine form 1 at 90K [45] and at RT [44] determined by the crystallographic methods differ insignificantly (by  $92.5 \text{ \AA}^3$  in volume;  $V(90 \text{ K})=3032.5$  and  $V(\text{RT})=3126 \text{ \AA}^3$ ), which suggests that no phase transition takes place over this range of temperatures. Because in clioquinol and cloxiquine there is only one type of each (nitrogen, oxygen, chlorine or iodine) site, thus the assignment of the NQR frequencies to particular sites is obvious. The differences in the reproduced NQR parameters for forms I and II of cloxiquine, Table 2, are large enough for unambiguous identification of the present polymorphic form as form I. This conclusion can be justified by two factors: significant differences between  $e^2Qq/h$  and  $\eta$  especially at  $^{17}\text{O}$  site for both forms, Table 2, and what is more important by a much better correlation between experimental and DFT calculated  $^{14}\text{N}$  and  $^{17}\text{O}$  NQR frequencies (correlation coefficient and curve fit standard errors are: for form I 0.997 and 0.025MHz at RT, 0.9956 and 0.036 MHz at 90K, but for form II only 0.986 and 0.105 MHz), Fig. 5a. It is worth noting that the NQR frequency at  $^{35}\text{Cl}$  site is less useful. Although it is more sensitive to the influence of temperature than those at  $^{17}\text{O}$  and  $^{14}\text{N}$  sites, but  $^{35}\text{Cl}$  site is distinct and thus less sensitive to the structural changes in the stacked dimers.

Surprisingly, the NQR parameters for clioquinol are better reproduced when assuming the X-Ray structure from [43] denoted as form Ia, than that from [42] denoted as form Ib, Table 3, which suggests that the first structure is better resolved, however residual factor given by the authors for this structure is only 10% in comparison to 8.4% for the second structure. The NQR parameters:  $e^2Qq/h^{-1}$ ,  $\eta$  and frequencies at all quadrupolar nuclei were calculated at the B3LYP/6-311++G(d,p) level assuming X-Ray data for clioquinol and cloxiquine (both polymorphic forms) and different molecular aggregations (monomer, dimer, stacked dimers) formed by the

intermolecular interactions. The results are collected in Table 2. The orientation of the principal axes of the EFG tensors at each site is shown in Fig. 6a-6c. The good accuracy of reproduction of the  $e^2Qqh^{-1}$ ,  $\eta$  and NQR frequencies at all quadrupolar nuclei  $^{14}\text{N}$ ,  $^{17}\text{O}$  and  $^{35}\text{Cl}$  at chosen DFT level (correlation coefficient as high as 0.999, and curve fit standard errors as low as 0.38 MHz), requires assumption of the optimized proton positions and taking into account the intermolecular bondings, Tables 2 and 3, Fig. 5b, which is in a good agreement with the results of our previous studies of purines [23, 24] or polyhalogenobenzimidazoles [25]. Besides  $e^2Qqh^{-1}$  and  $\eta$ , another criterion for checking the quality of reproduction of the EFG tensor by DFT is a comparison of orientation of its principal axes following from DFT as well as  $-\text{OH}$  bond length with those obtained from the experimental  $^{17}\text{O}$  spectrum. The orientation of the  $z$  axis of EFG tensor determined from  $^{17}\text{O}$  for cloxiquine is in a good agreement with the result of DFT calculations. DFT suggest that the O-H bond, which according to NQDR results lies in the X-Z plane of the EFG tensor, deviates from the X-Z plane only by 3deg and makes  $44\pm 1$  deg angle with the  $z$ -axis of EFG tensor, while the experiment suggests  $\theta = 50 \pm 5$  deg. The source of this slight discrepancy can be the neglect of other interactions taking place besides the hydrogen bondings. The  $-\text{OH}$  bond length,  $R(\text{O-H})$ , determined by  $^{17}\text{O}$  NQDR for cloxiquine is  $R(\text{O-H}) = (0.99 \pm 0.02)$  Å i.e. in a good agreement with the X-Ray data at 90K [45] and DFT partial optimization result for a monomer 0.987 Å and dimer 1.011 Å. The O-H bond length for clioquinol obtained from partial DFT optimization  $R(\text{O-H}) = 0.992$  Å is also much higher than those given in the ref. [42] i.e. 0.728 Å. The change in  $\angle\text{OHN}$  angle describing the linearity of the  $\text{O-H}\cdots\text{N}$  bond influences considerably the NQR parameters, even more than the changes in its length, which explains better reproduction of the NQR parameters for the structure with the optimized proton positions.

## Structural pattern

### *Supramolecular synthon*

According to the crystallographic data, the hydrogen bonding patterns in solid clioquinol and cloxiquine (form I) [42-45] are isostructural to those in the parent 8-quinolinol [46]. The hydroxyl hydrogens are capable of forming multicenter bonds i.e. bifurcated  $\text{O-H}\cdots\text{N}$  hydrogen bonds, one intramolecular and the other intermolecular, which simultaneously

lead to formation of five-membered hydrogen-bonded chelate rings [N, C(9), C(8), O, H(8)] and to dimerization of the molecules, respectively, as indicated in Fig. 7a-7c. Such patterns, usually termed supramolecular synthons [47], according to the X-ray data are independent of the polymorphic form, however in the dimeric structure of clioquinol (form I) and cloxiquine (form I a,b) the paired molecules in the units are twisted while in cloxiquine (form II) they are not. Due to this subtle difference in the planarity of the dimeric structures which consist of the paired molecules linked by bifurcated hydrogen bonds in the units (twisted in form I, and planar in form II) [44, 45], accompanied by a change in the hydrogen bond lengths, in cloxiquine the structural units can be differently packed to yield two polymorphs. As follows from X-Ray data, the intramolecular hydrogen bonds O-H...N in clioquinol ( $R_{O-H...N}=2.753$  [42] or  $2.818 \text{ \AA}$  [43]) are longer than those reported in cloxiquine ( $R_{O-H...N}=2.811$  [44] and  $2.747 \text{ \AA}$  [45]), both close to those in 8-quinolinol ( $R_{O-H...N}=2.753 \text{ \AA}$  [46]). The intermolecular hydrogen bonds O-H...N in clioquinol form Ia ( $R_{O-H...N}=2.792$ ) are shorter than those reported in cloxiquine ( $R_{O-H...N}=2.859$  and  $2.833 \text{ \AA}$ ), but similar to those in 8-quinolinol ( $R_{O-H...N}=2.793 \text{ \AA}$ ), while in clioquinol form Ib they ( $R_{O-H...N}=2.850$ ) are close to those reported in cloxiquine and much longer than those reported in 8-quinolinol ( $R_{O-H...N}=2.793 \text{ \AA}$ ). The intramolecular hydrogen bonds in clioquinol and cloxiquine are much more nonlinear ( $\angle OHN=87$  (form Ia) or  $95 \text{ deg}$  (form Ib) and  $108 \text{ deg}$  (form I) or  $115 \text{ deg}$  (form II), for clioquinol and cloxiquine, respectively versus  $109 \text{ deg}$  in 8-quinolinol) than the intermolecular ones ( $\angle OHN=151.5$  and  $151.8 \text{ deg}$  versus  $146.1$  and  $127.5 \text{ deg}$  versus  $143.0 \text{ deg}$  in 8-quinolinol).

The hydrogen bonds were characterized within the Bader QTAIM theory describing their molecular topology in terms of BCP and RCP. The topological parameters (bond length  $r$ , electron density  $\rho$ , its Laplacian  $\Delta\rho$ , ellipticity  $\varepsilon$ , BCP and RCP) are collected in Table 3 and describe the molecular stability and characterize the internuclear pathways, which can be classified as shared or closed-shell. All the expected BCPs associated with the standard covalent bonds and RCPs at the centroid of all benzenoid rings were found in monomers and dimers of both compounds. In addition, in monomer one extra BCP was found assigned to weak intramolecular interaction, which in turn generate one more ring RCP, but exclusively in cloxiquine form II. The presence of RCP and BCP in the monomer of cloxiquine form II confirms the existence of intramolecular O-H...N hydrogen bond since the topological criteria proposed by Koch and Popelier [48] are fulfilled. Surprisingly, in contrast to cloxiquine form II, the lack of BCP between the putative donor and the acceptor in monomer of cloxiquine form I or clioquinol form I, implies no O-H...N hydrogen bond, which suggests that if there is this

interaction at all - it is very weak and repulsive rather than attractive. The presence of RCPs in five-membered hydrogen-bonded chelate rings and the presence of BCPs in both kinds of hydrogen bonds in supramolecular synthon of cloxiquine form II, Table 3, confirms the existence of different kinds of H-bonds: intramolecular O-H...N and intermolecular O-H...N and C-H...O in cloxiquine form II in contrast to the occurrence of only intermolecular O-H...N in the structures of cloxiquine and clioquinol form I.

For supramolecular synthon of cloxiquine or clioquinol form I, similarly as for monomer, there is no evidence of intramolecular H-bond O-H...N, which suggests that the geometric criteria are insufficient for the existence of hydrogen bonding. Additionally, the very weak intermolecular halogen contacts Cl...I ( $\text{Cl}\cdots\text{I}=3.710 \text{ \AA}$ ) and hydrogen bonds C-H...I ( $R_{\text{C-H}\cdots\text{I}}=4.026 \text{ \AA}$ ) were revealed in the structure of clioquinol, but only in form Ib. The QTAIM calculations yielded the value of electron densities of 0.019 a.u. for intramolecular bonds and 0.020-0.034 a.u. for intermolecular ones (it falls within a certain range of values, typically between 0.001 and 0.035 a.u.) markedly lower than for the covalent bonds. The corresponding Laplacian values,  $\Delta\rho$ , are positive and amount to 0.08 a.u. and 0.04-0.09 a.u. (typically between 0.006 and 0.130 a.u.) which is indicative of the closed-shell interaction. The relief maps of the Laplacian of electron density for clioquinol and cloxiquine in the plane of intermolecular H-bond O-H...N, Fig. 8a-8c, exhibits a maxima in the negative Laplacian on either side of the oxygen and nitrogen atoms, corresponding to the lone pair model. Moreover, they show the polarization of the nitrogen lone-pair electrons toward hydrogen and differences in polarization of the oxygen and nitrogen lone-pairs caused by the changes in planarity as well as iodine substitution.

To get further insights into the nature of intermolecular and intramolecular interactions, electronic energy density  $H_{\text{BCP}}$  and its components, the local one electron kinetic energy density ( $G_{\text{BCP}}$ ), and the local potential energy density ( $V_{\text{BCP}}$ ), for the charge distribution at the BCP were calculated. The hydrogen and halogen bond energies were calculated using CP as well as according to the Espinosa method, Table 3. According to Rozas [49] criterion, the intramolecular O-H...N bonds in cloxiquine form II are weak and slightly stronger than the intermolecular O-H...N bonds, Table 3, but generally weaker than typical and mainly electrostatic, while the intermolecular O-H...N bonds in clioquinol and cloxiquine form I at RT are moderate and partially covalent in nature. The estimated H-bond energies for the systems studied lie within the range of 8.33-34.39  $\text{kJ mol}^{-1}$ , Table 3. Partitioning of DFT energy of the hydrogen bond into

classical components showed that about 75% was electrostatic (Coulombic) and less than 5% came from polarization and charge-transfer.

The large differences in the strength of the corresponding H-bonds in both cloxiquine forms, suggests the interplay between different H-bonds in adjacent molecules creating dimers. It is worth noting that the energies of the H-bonds in cloxiquine form I estimated by the Espinosa method seem reasonably higher at 90K than those at RT (about  $5.6 \text{ kJ mol}^{-1}$ ) when the non-optimized structures are taken into account. Moreover, the additional weak intermolecular contact between nitrogen atoms is detected, but only when an extra short OH bond taken from X-Ray data at RT is assumed. On the other hand, the hydrogen bond energies for clioquinol forms Ia and Ib differ by as much as  $6.5 \text{ kJ mol}^{-1}$ , however both structures were determined at RT and the difference in the relevant R factors is only 1.6%. It should be mentioned that the estimation of H-bond energy according to Espinosa should be used only for comparisons of the strength of H-bonds but should not be considered quantitatively.

As follows from QTAIM results, the intermolecular hydrogen bonds O-H...N in cloxiquine and clioquinol (form I), are the strongest interactions, which is in agreement with the previous suggestions based on the differences in the hydrogen acceptor distances [50] as well as the IR spectra in solution [51]. In clioquinol, additional electron-withdrawing substituent (iodine) *ortho* to the hydroxyl group is competitive to chlorine in *para* and results in the formation of stronger hydrogen bond than those in cloxiquine, which is consistent with the IR spectra in solid (KBr). The direction of the spectral shifts of the O-H stretch mode in the mid-infrared, often used to infer the strength of the hydrogen bond, is in a good agreement with the DFT results, Table 3a,b. Proton donor and acceptor sites in hydrogen bonds in supramolecular synthons in solid can be reliably characterized using  $^1\text{H}$ - $^{17}\text{O}$  and  $^1\text{H}$ - $^{14}\text{N}$  NQDR spectroscopy. It should be noted that the calculations revealed that the presence of the intermolecular O-H...N hydrogen bonding influences NQR parameters differently at different sites, only slightly for  $^{35}\text{Cl}$  i.e. at the site distant from hydrogen bond, while significantly at  $^{17}\text{O}$  and  $^{14}\text{N}$  both participating in this bond; a comparison of the experimental data and the results of calculations for the monomer and stacked dimers, Table 3, is a drastic example.

The electron withdrawing iodine substituent at position 7 of 5-chloro-8-quinolinol results in a decrease in the proton affinity of nitrogen atom and an increase in the hydrogen bond strength, which induces changes in the values of  $e^2\text{Qqh}^{-1}$  and  $\eta$ , Tables 1 and 2.

As a result of substitution,  $e^2Qqh^{-1}$  increases on  $^{35}\text{Cl}$  and  $^{14}\text{N}$  by 0.01 and 2%, respectively, while on  $^{17}\text{O}$  this parameter is predicted to decrease by 0.05%. The predicted changes in  $\eta$  on  $^{35}\text{Cl}$  are negligibly small, on  $^{17}\text{O}$  this parameter decreases by 3%, but on  $^{14}\text{N}$  it increases by 2%. The direction of changes in NQR parameters observed upon change from cloxiquine to clioquinol is in agreement with the Seliger's [52] observation that on shortening and hence also strengthening of the hydrogen bond, the asymmetry parameter  $\eta$  increases. A considerable increase in  $e^2Qqh^{-1}$  on the chlorine atom, which implies a decrease in the symmetry of charge distribution at this atom towards non-spherical symmetry, is also observed mainly as a consequence of iodine electron-withdrawing substituent *ortho* to the chlorine. Comparison of the results obtained for clusters of different size, Table 2, shows that the value of  $e^2Qqh^{-1}$  depends strongly on the presence of hydrogen bonding and that  $\eta$  can be used as an indicator of the strength of the hydrogen bonding.

Because of quite a short proton distance (2.182 and 2.622 Å) in the structures of cloxiquine and clioquinol, the O-H...H-O dihydrogen bonds could be expected, besides the HB intermolecular interactions. The H...H distance of less than 2.4 Å i.e. twice the van der Waals radius of hydrogen atom (1.2Å) is the most widely used so-called geometrical criterion to identify formation of this type hydrogen bonds. However, because the dihydrogen bondings are electrostatic in nature and such interactions acts beyond this distance, van der Waals criterion is strongly criticized [53]. The additional criteria taken into account are: the interaction energy (which falls within the same range of typically hydrogen bonds, 12–41 kJ mol<sup>-1</sup>), the linearity of dihydrogen bonds and the difference in charges on both electronegative atoms [54, 55]. QTAIM does not detect the critical points indicating the presence of the O-H...H-O dihydrogen bond for any form of clioquinol as well as cloxiquine, which seems to be a consequence of the same polarization of both oxygen atoms forced by the symmetric dimeric structure.

### *Stacked supermolecular synthon*

An important type of interactions specific of the solid state commonly seen in aromatic systems is the vertical stacking of parallel supramolecular synthons, Fig. 9a-9c. As mentioned earlier, in the dimeric structure of clioquinol and cloxiquine (form I) the paired molecules in the units are twisted and the units expand into columns linked by  $\pi$ - $\pi$  stacking interaction with distinct layers distanced by only 3.814 Å in cloxiquine [45] (i.e. close to 3.811 Å observed in 8-quinolinol [46]) and as large as 4.141 or 4.161 Å in clioquinol [42, 43], which suggests large steric repulsion

coming from I-I, forcing larger spacing between layers. The difference between forms I and II of cloxiquine, Fig. 9a, 9b, is that the twisted and non-twisted adjacent supramolecular synthons form columns along different crystallographic axes (c in Form I and b in Form II) [45]. The  $\pi$ - $\pi$  stacking interactions between adjacent supramolecular synthons (stacked dimers) enhance the stability in the crystal structures of both clioquinol and cloxiquine, irrespective of the specific polymorph; however their strength is expected to differ because of great differences in the polarization of the adjacent molecules and so also dimers responsible for the specific arrangement in parallel columns.

The dipole moments calculated by DFT method for a continuous distribution of electron density provide essential information on the overall polarity of the charge system. The monomer of clioquinol has higher dipole moment than that of cloxiquine form I (3.15 (from Ia) or 3.20 (form Ib) or versus 1.71 D (form I, RT)), while the dimer and stacked dimers have lower dipole moments (3.97 (form Ia), 3.94 (form Ib) versus 1.97 D and 3.07 (form Ia) and 3.03 (form Ib) versus 4.14 D (form I, RT), for clioquinol and cloxiquine, respectively). Moreover, in form II of cloxiquine, which is predicted to be energetically more stable than form I (by 13.6 kJ mol<sup>-1</sup>), the monomer has slightly higher dipole moment (1.82 D), while the dimer and stacked dimers are non-polar (0.02 and 0.005 D, respectively), which suggest great differences in the polarization of the adjacent molecules so that dimers are closely connected with the specific arrangement. The stacking found in clioquinol and cloxiquine (form I) involves similar overlapping, however much smaller than observed in cloxiquine (form II). The nucleus independent chemical shift (NICS) calculated at the geometrical center and its modification NICS(1) calculated at 1°A above the plane of the ring, both reflecting  $\pi$  effects, are negative, which means that the Schleyer *et al.* [56] criterion of aromaticity is fulfilled for both compounds irrespective the form. The standard method of estimation of the energy of stacking  $\pi$ ··· $\pi$  interactions (CP), seems to be ineffective for such a complicated system. The roughly estimated energy of  $\pi$ - $\pi$  stacking interactions is as high as 16.3 and 14.5 kJ mol<sup>-1</sup> for clioquinol forms Ia and Ib, respectively, 19.8 and 23.6 kJ mol<sup>-1</sup> for cloxiquine form I and form II, respectively. The comparison of energy suggests that the strength of stacking  $\pi$ ··· $\pi$  interaction depends on planarity i.e. is much weaker in form I than form II of cloxiquine and that the lower energy of  $\pi$ - $\pi$  stacking for clioquinol in comparison to cloxiquine results from larger spacing between layers.

More detailed examination of the closest-neighbor stacked supramolecular synthons revealed one intermolecular hydrogen bond C-H···O (only cloxiquine form I; clioquinol forms Ia, Ib) and

five unique intermolecular atomic contacts (all forms) in addition to intermolecular bonds revealed earlier in the crystal packing of both compounds, Fig. 9. According to the topological parameters reported in Table 4, all these intermolecular interactions analyzed here are weak except the intermolecular O-H...N hydrogen bonds. The topology of these weak intermolecular interactions, which are characterized by very small values of  $\rho(r)$ , small positive values of Laplacian, high values of  $\varepsilon$  and nearly zero values of  $H_{\text{BCP}}$  and values of  $|V_{\text{BCP}}/G_{\text{BCP}}| \leq 1$ , Table 4, was analysed using QTAIM. In terms of the Espinosa classification [41] these interactions fall between the pure closed-shell and transit type. The energy of these weak interactions depends linearly on the electron density at the critical point and the Laplacian of density, Fig.10a, 10b. The high values of ellipticity are connected with the relatively low value of the second hessian eigenvalue and thus the presence of RCP besides BCP cannot be ascribed to  $\pi$  bonding.

As follows from a comparative analysis of BCPs and RCPs of cloxiquine form I and form II, in form I there is one hydrogen bond O-H...N, while in form II there are two competing hydrogen bonds O-H...N intra and intermolecular (the former is somewhat stronger than the latter), Table 4. Moreover, the intermolecular C-H...O in form I links the molecules from the same supramolecular synthon, Fig. 9a, while in form II it links the molecules from different (stacked) supramolecular synthons, Fig. 9b and is much (almost twice) weaker. Such a pattern of bonds induces the planarity of the supramolecular synthons in cloxiquine form II and it is also responsible for the differences in polarity of the supramolecular synthons in cloxiquine form I and II. The ellipticity of all covalent bonds in which nitrogen and oxygen atoms participate does not change significantly in both forms of cloxiquine. Hence, we may conclude that the planarity does not force  $\pi$ -electron delocalization within the quinolinol ring. The large change in ellipticity at BCP of N...O bond suggests that the planarity forces  $\pi$ -electron delocalization in pseudo deca-membered ring. The H-bonds energies listed in Tables 3 and 4, i.e. for all supramolecular synthons and stacked supramolecular synthons are very well correlated, Fig. 10c and the differences between them do not exceed  $0.19 \text{ kJ mol}^{-1}$ , which means that there are no interplay between H-bonds in adjacent molecules creating supramolecular synthons and intermolecular interactions between stacked supramolecular synthons. Additionally, Fig. 11a illustrates a good and parabolic relationship between the H...Y distance and the estimated hydrogen bond energy  $E_E$ . The electron density and the Laplacian of density at BCP of H...Y contact depend exponentially and linearly on the H...Y distance, respectively, Fig. 11b and Fig. 11c. It is worth noting that the points in Figs. 10 and 11 for dimer and stacked dimer overlap, thus only one set (the second case) is shown, which confirms the lack of interplay between H-bonds in adjacent

molecules creating dimers and intermolecular interactions between stacked dimers. It should be emphasized that these dependencies characterizing H-bonds, Figs. 10c and 11a-c, observed for H-bonds in stacked supramolecular synthons are in excellent agreement with the results previously reported by Espinosa but obtained only for small molecular systems [41].

The pattern of the intra and intermolecular interactions in clioquinol form I (Ia and Ib) is generally similar to that observed for cloxiquine form I, Table 4, Figs. 7-11, however the smaller number of weak interactions between the carbon atoms from heterocyclic rings (2 versus 4) and the appearance of two (form Ia) or three (form Ib) weak interactions coming from I contacts should be indicated. The ellipticity of all (covalent and hydrogen) bonds, in which nitrogen and oxygen atoms participate, increases significantly in clioquinol in comparison to cloxiquine. Hence, we may conclude that the electron withdrawing substituent do influence  $\pi$ -electron delocalization within the quinolinol ring and pseudo deca-membered ring. According to our experimental and theoretical results, the oxygen atom is much more sensitive to the differences in planarity of the supramolecular synthons than the nitrogen atom involved in the same O-H...N bond. The considerable differences in the NQR parameters for the planar and twisted supramolecular synthons, permit differentiation between the specific polymorphic forms and suggest the presence of form I in both experimentally studied samples.

## Conclusions

1. The NQR parameters  $e^2Qqh^{-1}$  and  $\eta$  at O site indicate the differences in the planarity of the supramolecular synthons and thus enable differentiation between the polymorphic forms. This conclusion can be derived on the basis of much better correlation between experimental and calculated by DFT NQR frequencies form form I than form II.
2. The results of QTAIM analysis suggest the interplay between different H-bonds in adjacent molecules creating dimers, but no interplay between H-bonds in adjacent molecules creating dimers and weak intermolecular interactions between stacked dimers.
3. The pattern of the intra and intermolecular interactions in clioquinol form Ia and Ib is generally similar to that observed for cloxiquine form I. The presence of I (iodine) substituent at C(7) position is crucial because thanks to this substituent clioquinol is able to form stronger

hydrogen bonds and reduce the number of weak interactions between the carbon atoms from heterocyclic rings. Moreover the electron withdrawing substituent (iodine) influences  $\pi$ -electron delocalization within the quinolinol ring and pseudo deca-membered ring, which can be easily observed as a change in NQR parameters at N and O atoms.

4. A comparison of the results for monomer, dimer and cluster (stacked dimers) shows systematic improvement in the reproduction of NQR parameters to a degree proportional to the strength of the interactions (the weaker the interaction the smaller the correction).

### **Acknowledgments**

Generous allotment of computer time from the PCSS (Poznań Supercomputing and Networking Centre), Poland is gratefully acknowledged.

## References

1. Rohde W, Mikelens P, Jackson J, Blackman J, Whitcher J, Levinson W (1976) *Antimicrob Agents Chemother* 10:234-240
2. Fischer T, Fagerlund C, Hartvig P (1978) *Acta DermVenereol* 58:407-411
3. Gholz LM, Arons WL (1964) *Am J Trop Med Hyg* 13:396-401
4. Compendium of pharmaceuticals and specialties (1991) Canadian Pharmaceutical Association Ottawa, Ed Krogh CME p 1311
5. Oradell NJ (1991) *Physicians' desk reference*. Medical Economics Company p 874
6. Burger A (1970), *Medicinal chemistry*, 3<sup>rd</sup> ed. John Wiley & Sons, New York, NY
7. Yassin MS, Ekblom J, Xilinas M (2000) *J Neurol Sci* 173:40-44
8. Kaiser HJ, Kunze J (1982) *Zubereitungen Fortschr Ther* 100:1265-1267
9. Hongmanee P, Rukseree K, Buabut B, Somsri B, Palittapongarnpim P (2007) *Antimicrob Agents Chemother* 51:1105-1106
10. Thomas PK, Bradley DJ, Bradley WA, Degen PH, Krinke G, Muddle J, Schaumburg HH, Skeltonstroud PN, Thomann P, Tzebelikos E (1984) *J Neurol Sci* 64:277-295
11. Tjälve H (1984) *Medical Hypotheses* 15:293-299
12. Baumgartner G, Gawel HE, Pallis CA, Clifford F, Schaumburg HH, Thomas PK, Wadia NH (1979) *J Neurol Neurosurg Psychiatry* 42:1075-1083
13. Ricoy RJ, Ortega A, Cabello A (1982) *J Neurol Sci* 53:241-251
14. Nguyen T, Hamby A, Massa SM (2005) *Proc Natl Acad Sci USA* 102:11840-11845
15. Ritchie CW, Bush AI, Masters CL (2004) *Expert Opin Investig Drugs* 13:1585-1592
16. Cherny RA, Atwood CS, Xilinas ME, Gray DN, Jones WD, McLean CA, Barnham KJ, Volitakis I, Fraser FW, Kim Y, Huang X, Goldstein LE, Moir RD, Lim JT, Beyreuther K, Zheng H, Tanzi RE, Masters CL, Bush AI (2001) *Neuron* 30:665-676
17. Ritchie CW, Bush AI, Mackinnon A, Macfarlane S, Mastwyk M, MacGregor L, Kiers L, Cherny R, Li QX, Tammer A, Carrington D, Mavros C, Volitakis I, Xilinas M, Ames D, Davis S, Beyreuther K, Tanzi RE, Masters CL (2003) *Arch Neurol* 60:1685-1691
18. Wang Y, Branicky R, Stepanyan Z, Carroll M, Guimond MP, Hiji A, Hayes S, K McBride, Hekimi (2009) *J Biol Chem* 284:314-323
19. Mao X, Li SX, Sprangers R, Wang X, Venugopal A, Wood T, Zhang Y, Kuntz DA, Coe E, Trudel S, Rose D, Batey RA, Kay LE, Schimmer AD (2009) *Leukemia* 23:585-590
20. Ding WQ, Liu B, Vaught JL, Yamauchi H, Lind SE (2005) *Cancer Research* 65:3389-3395
21. Latosińska JN (2005) *J Mol Graph Model* 23:329-337

22. Latosińska JN (2007) *Expert Opinion On Drug Discovery* 2:225-248
23. Latosińska JN, Latosińska M, Seliger J, Žagar V, Kazimierczuk Z (2009) *Chem Phys Lett* 476:293-302
24. Latosińska JN, Seliger J, Žagar V, Burchardt DV (2009) *J Phys Chem A* 113:8781-8790
25. Latosińska JN, Latosińska M, Seliger J, Žagar V, Maurin JK, Orzeszko A, Kazimierczuk Z (2010) *J Phys Chem A* 114:563-575
26. Seliger J (2000) In: Lindon JC, Tranter GE, Holmes JL (eds) *NQR Theory in Encyclopedia of Spectroscopy and Spectrometry*. pp 1672-1680
27. Seliger J, Osredkar R, Mali M, Blinc R (1976) *J Chem Phys* 65:2887-2891
28. Seliger J, Blinc R, Arend H, Kind R (1976) *Z Phys B* 25:185-189
29. Stephenson D, Smith JAS (1988) *Proc R Soc Lond A* 416:149-178
30. Seliger J, Žagar V (2008) *J Magn Reson* 193:54-62
31. Seliger J, Žagar V, Blinc R (1994) *J Magn Reson, A* 106:214-222
32. Slusher RE, Hahn EL (1968) *Phys Rev* 166: 332-347
33. Seliger J, Žagar V (2008) *J Magn Reson* 194:175-181
34. Brosnan SGP, Edmonds DT (1981) *J Magn Reson* 45:440-450
35. Seliger J, Žagar V, Blinc R, Novak A (1986) *J Chem Phys* 84:5857-5861
36. Frisch MJ, Trucks GW, Schlegel HB, Scuseria GE, Robb MA, Cheeseman JR, Montgomery JA Jr, Vreven T, Kudin KN, Burant JC, Millam JM, Iyengar SS, Tomasi J, Barone V, Mennucci B, Cossi M, Scalmani G, Rega N, Petersson GA, Nakatsuji H, Hada M, Ehara M, Toyota K, Fukuda R, Hasegawa J, Ishida M, Nakajima T, Honda Y, Kitao O, Nakai H, Klene M, Li X, Knox JE, Hratchian HP, Cross JB, Bakken V, Adamo C, Jaramillo J, Gomperts R, Stratmann RE, Yazyev O, Austin AJ, Cammi R, Pomelli C, Ochterski JW, Ayala PY, Morokuma K, Voth GA, Salvador P, Dannenberg JJ, Zakrzewski VG, Dapprich S, Daniels AD, Strain MC, Farkas O, Malick DK, Rabuck AD, Raghavachari K, Foresman JB, Ortiz JV, Cui Q, Baboul AG, Clifford S, Cioslowski J, Stefanov BB, Liu G, Liashenko A, Piskorz P, Komaromi I, Martin RL, Fox DJ, Keith T, Al-Laham MA, Peng CY, Nanayakkara A, Challacombe M, Gill PMW, Johnson B, Chen W, Wong MW, Gonzalez C, Pople JA (2004) *Gaussian 03, Revision D01*. Gaussian Inc, Wallingford CT
37. Becke AD (1993) *J Chem Phys* 98:1372-1377
38. Lee C, Yang W, Parr RG (1988) *Phys Rev B* 37:785-789
39. Bader RFW (1994) *Atoms in Molecules: A Quantum Theory*, Oxford University Press
40. Boys SB, Bernardi F (1970) *Mol Phys* 17:553-566
41. Espinosa E, Molins E, Lecomte C (1998) *Chem Phys Lett* 285:170-173

42. Kashino S, Haisa M (1973) *Bull Chem Soc Jpn* 46:1094-1098
43. Leger JM, Marsau P, Housty J (1972) *C R Acad Sci, Ser C (Chim)* 274:1991
44. Banerjee T, Saha NN (1986) *Acta Crystallogr, Sect C: Cryst Struct Commun* 42:1408-1411
45. Ma Z, Moulton B (2009) *J Chem Cryst* 39:913-918
46. Roychowdhury P, Das BN, Basak BS (1978) *Acta Cryst B* 34:1047-1048
47. Desiraju GR (1994) *Angew Chem Int* 34:2311-2327
48. Koch PLA, Popelier A (1995) *J Phys Chem* 99:9747-9754
49. Rozas, Alkorta I, Elguero J (2000) *J Am Chem Soc* 122:11154-11161
50. Ceccarelli C, Jeffrey GA, Taylor R (1981) *J Mol Struct* 70:255-271
51. Badger GM, Moritz AG (1958) *J Chem Soc* 3437-3442
52. Seliger J (1998) *Chem Phys* 231:81-86
53. Desiraju GR, Steiner T (1999) *The Weak Hydrogen Bond in Structural Chemistry and Biology*. Oxford University Press, New York
54. Grabowski SJ (2004) *J Phys Chem A* 108:5823-5830
55. Grabowski SJ, Sokalski WA, Leszczynski J (2005) *J Phys Chem A* 109:4331-4341
56. Schleyer PvR, Maercker C, Dransfield A, Jiao H, Hommes NJ, Hommes RE (1996) *J Am Chem Soc* 118:6317-6318

## Tables

**Table 1** The experimental NQR parameters for clioquinol and cloxiquine ( $^{35}\text{Cl}$  NQR frequency,  $^{14}\text{N}$  NQR frequencies  $\nu_+$ ,  $\nu_-$  and  $\nu_0$ ,  $^{17}\text{O}$  NQR frequencies  $\nu_{3/2-1/2}$ ,  $\nu_{3/2-1/2}$  and  $\nu_{3/2-1/2}$ , the widths  $\delta\nu_{3/2-1/2}$ ,  $\delta\nu_{3/2-1/2}$  and  $\delta\nu_{3/2-1/2}$  of the NQDR lines, the quadrupole coupling constants  $e^2qQ/h$  and the asymmetry parameters  $\eta$  of the EFG tensor, the proton-oxygen distance  $R(\text{O-H})$ , the angle  $\theta$  between the O-H bond and the principal axis Z of the EFG tensor and the angle  $\varphi$  between the projection of the O-H bond on the X-Y plane and the principal axis X of the EFG tensor)

COMPOUND	SITE	$\nu$ [MHz] ( $\delta\nu$ [kHz])	$e^2Qqh^{-1}$ [MHz]	$\eta$ [-]	$R(\text{O-H})$ [Å]	$\theta$	$\varphi$	T [K]
Cloxiquine	N	3.328 2.828 0.500	4.104	0.244	-	-	-	295
	O	4.175 (120) 2.425 (120) 1.750 (110)	8.610	0.622	0.99	50°	0°	213
	Cl	34.787 (21)	69.574 <sup>a</sup>	0	-	-	-	77
Clioquinol	N	3.407 2.831 0.575	4.159	0.276	-	-	-	295
	Cl	35.170 (22)	71.420 <sup>a</sup>	0	-	-	-	77

<sup>a</sup>calculated under assumption  $\eta=0$

**Table 2** The NQR parameters calculated calcu at the B3LYP/6-311++G(d,p) level of theory for different polymorphic forms of cloiquinol and cloxiquine

COMPOUND	FORM	SITE	MONOMER			DIMER			STACKED DIMERS		
			$\frac{V_{zz}V_{zz}V_0}{V_{S(2-1/2),V_{S(2-3/2)},V_{S(2-1/2)}} \nu$ [MHz]	$e^2Qqh^{-1}$ [MHz]	$\eta$ [-]	$\frac{V_{zz}V_{zz}V_0}{V_{S(2-1/2),V_{S(2-3/2)},V_{S(2-1/2)}} \nu$ [MHz]	$e^2Qqh^{-1}$ [MHz]	$\eta$ [-]	$\frac{V_{zz}V_{zz}V_0}{V_{S(2-1/2),V_{S(2-3/2)},V_{S(2-1/2)}} \nu$ [MHz]	$e^2Qqh^{-1}$ [MHz]	$\eta$ [-]
Cloxiquine	Form I RT [44] opt*	N	3.969 3.285 0.684	4.836	0.283	3.607 3.079 0.528	4.457	0.237	3.610 3.080 0.530	4.460	0.238
		O	5.116 2.907 2.208	10.424	0.680	4.717 2.764 1.953	9.776	0.599	4.732 2.757 1.974	9.766	0.614
		Cl	33.634	67.074	0.093	33.663	67.145	0.090	33.881	67.611	0.082
	Form I 90K [45] opt*	N	4.007 3.310 0.698	4.878	0.286	3.860 3.251 0.609	4.741	0.257	3.881 3.256 0.626	4.758	0.263
		O	4.838 2.730 2.108	9.817	0.699	4.621 2.644 1.977	9.453	0.662	4.635 2.639 1.996	9.452	0.676
		Cl	34.005	67.859	0.082	33.987	67.826	0.081	34.224	68.330	0.072
	Form II 90K [45] opt*	N	3.884 3.202 0.683	4.724	0.289	3.666 3.084 0.583	4.500	0.259	3.706 3.100 0.606	4.537	0.267
		O	4.802 2.547 2.256	9.402	0.855	4.568 2.437 2.131	8.975	0.840	4.528 2.405 2.123	8.981	0.834
		Cl	34.038	67.928	0.081	34.030	67.918	0.079	34.195	68.273	0.072
Cloiquinol	Form I [43] opt*	N	4.06 3.41 0.64	4.979	0.259	3.71 3.22 0.49	4.621	0.210	3.69 3.21 0.47	4.602	0.206
		O	5.189 2.866 2.424	10.403	0.754	4.830 2.781 2.049	9.915	0.646	4.836 2.765 2.072	9.886	0.665
		Cl	34.372	68.566	0.088	34.413	68.657	0.086	34.589	69.012	0.085
		I	889.136 585.596 303.540	1971.039	0.104	886.267 587.800 298.467	1964.244	0.109	894.756 594.783 299.972	1985.258	0.082
	Form I [42] opt*	N	4.06 3.53 0.52	5.062	0.207	3.70 3.34 0.36	4.692	0.154	3.69 3.33 0.36	4.680	0.152
		O	5.033 2.834 2.199	10.202	0.704	4.674 2.732 1.941	9.673	0.605	4.686 2.716 1.969	9.654	0.628
		Cl	35.335	70.551	0.071	35.382	70.655	0.068	35.539	70.975	0.066
		I	897.710 596.647 301.062	1991.812	0.084	895.961 597.043 300.708	1987.492	0.089	903.91 601.23 302.673	2007.117	0.060

\* partially optimized geometry

**Table 3a** Topological parameters of  $\rho$  for the supramolecular synthons of cloxiquine (the electron density at BCP and RCP ( $\rho$ ), its Laplacian  $\Delta(\rho)$ , the potential electron energy density ( $V_{BCP}$ ), the kinetic electron energy density ( $G_{BCP}$ ) and the total electron energy density ( $H_{BCP}$ ) and energy of interactions ( $E_{BSSE}$  or  $E_E$ ) calculated at the B3LYP/6-311++G(d,p) level of theory

COMPOUND	FORM	INTERACTION/CRITICAL POINT TYPE	$E_{BSSE}$ [kJ/mol]	$R(X\cdots Y)^{**}$ [Å]	$R(Y\cdots H)^{***}$ [Å]	$\rho$ [a.u.]	$\Delta(\rho)$ [a.u.]	$\varepsilon$ [-]	$G_{BCP}$ [a.u.]	$V_{BCP}$ [a.u.]	$H_{BCP}$ [a.u.]	$E_E$ [kJ/mol]	STRENGTH
Cloxiquine	Form I RT [44] R=4.9%	O-H...N intermolecular	-	2.858	1.934 (0.770)	0.0172	0.0711	0.0459	0.0149	-0.0119	0.0029	-15.68	weak
		N...N	-	3.373	-	0.0072	0.0202	0.9228	0.0045	-0.0039	0.0006	-5.07	-
		RCP CCOHNCCOHN intermolecular	-	-	-	0.0070	0.0210	-	0.0046	-0.0039	0.0007	-	-
		RCP benzene ring	-	-	-	0.0209	0.1519	-	0.0306	-0.0232	0.0074	-	-
		RCP heterocyclic ring	-	-	-	0.0240	0.1727	-	0.0356	-0.0281	0.0076	-	-
	Form I RT [44] opt <sup>*</sup>	O-H...N intermolecular	-35.75	2.859	1.934 (1.017)	0.0301	0.083	0.038	0.021	-0.021	-0.0002	-27.90	moderate
		RCP CCOHNCCOHN intermolecular	-	-	-	0.0090	0.026	-	0.035	-0.005	0.0306	-	-
		RCP benzene ring	-	-	-	0.0207	0.151	-	0.030	-0.023	0.0074	-	-
		RCP heterocyclic ring	-	-	-	0.0239	0.172	-	0.035	-0.028	0.0076	-	-
	Form I 90K [45]	O-H...N intermolecular	-9.42	2.811	2.063 (0.911)	0.0230	0.079	0.046	0.018	-0.016	0.0019	-21.07	weak
		RCP CCOHNCCOHN intermolecular	-	-	-	0.0086	0.025	-	0.005	-0.005	0.0007	-	-
		RCP benzene ring	-	-	-	0.0208	0.152	-	0.030	-0.023	0.0074	-	-
		RCP heterocyclic ring	-	-	-	0.0233	0.167	-	0.034	-0.027	0.0074	-	-
	Form II 90K [45]	O-H...N inter	-14.55	2.833	2.131 (0.982)	0.0203	0.068	0.021	0.015	-0.013	0.0019	-17.41	weak
		C-H...O inter		2.999	2.471 (0.949)	0.0089	0.041	0.609	0.008	-0.006	0.0019	-8.33	weak
		O-H...N intra	-	2.742	2.181 (0.982)	0.0198	0.077	0.928	0.017	-0.015	0.0022	-19.50	weak
		RCP O-H...N intramolecular NHOC	-	-	-	0.0195	0.098	-	0.021	-0.017	0.0038	-	-
		RCP intramolecular (CH...O) NCHOH	-	-	-	0.0086	0.046	-	0.009	-0.007	0.0022	-	-
		RCP CCOHNCCOHN O-H...N intermolecular	-	-	-	0.0072	0.020	-	0.004	-0.004	0.0008	-	-
		RCP benzene ring	-	-	-	0.0210	0.154	-	0.031	-0.024	0.0075	-	-
RCP heterocyclic ring		-	-	-	0.0235	0.169	-	0.035	-0.028	0.0074	-	-	

\* partially optimized geometry

\*\*  $R(X\cdots Y)$  donor (X) – acceptor (Y) distance

\*\*\*  $R(Y\cdots H)$  acceptor (Y) – proton (H) distance

**Table 3b** Topological parameters of  $\rho$  for the supramolecular synthons of clioquinol (the electron density at BCP and RCP ( $\rho$ ), its Laplacian  $\Delta(\rho)$ , the potential electron energy density ( $V_{BCP}$ ), the kinetic electron energy density ( $G_{BCP}$ ) and the total electron energy density ( $H_{BCP}$ ) and energy of interactions ( $E_{BSSE}$  or  $E_E$ ) calculated at the B3LYP/6-311++G(d,p) level of theory

COMPOUND	FORM	INTERACTION/CRITICAL POINT TYPE	$E_{BSSE}$ [kJ/mol]	$R(X\cdots Y)^*$ [Å]	$R(Y\cdots H)^{**}$ [Å]	$\rho$ [a.u.]	$\Delta(\rho)$ [a.u.]	$\varepsilon$ [-]	$G_{BCP}$ [a.u.]	$V_{BCP}$ [a.u.]	$H_{BCP}$ [a.u.]	$E_E$ [kJ/mol]	STRENGTH
Clioquinol	Form Ia RT [43] R=10%	BCP O-H...N intermolecular	-27.86	2.792	1.883 (0.986)	0.0340	0.094	0.041	0.025	-0.026	-0.0013	-34.39	moderate
		RCP O-H...N intermolecular	-	-	-	0.0102	0.030	-	0.007	-0.006	0.0009	-	-
		RCP benzene ring	-	-	-	0.0213	0.154	-	0.031	-0.024	0.0075	-	-
		RCP heterocyclic ring	-	-	-	0.0234	0.169	-	0.035	-0.027	0.0075	-	-
	Form Ib RT [42] R=8.4%	O-H...N intermolecular	-35.28	2.850	1.942 (0.988)	0.0297	0.084	0.045	0.021	-0.021	0.0001	-27.68	weak
		I...Cl	-1.88	3.710	-	0.0066	0.021	0.106	0.004	-0.0029	0.0012	-3.89	weak
		I...H-C		4.026	3.373 (0.653)	0.0045	0.013	0.161	0.003	-0.0019	0.0007	-2.49	weak
		RCP CCOHNCCOHN intermolecular	-	-	-	0.0089	0.026	-	0.006	-0.005	0.0008	-	-
		RCP CCCCIH	-	-	-	0.0037	0.012	-	0.002	-0.002	0.0001	-	-
		RCP benzene ring	-	-	-	0.0184	0.131	-	0.026	-0.019	0.0068	-	-
RCP heterocyclic ring	-	-	-	0.0215	0.152	-	0.031	-0.028	0.0031	-	-		

R – the reliability factor (R-factor)

\* $R(X\cdots Y)$  donor (X) – acceptor (Y) distance

\*\* $R(Y\cdots H)$  acceptor (Y) – proton (H) distance

**Table 4a.** Topological parameters of  $\rho$  for the stacked supramolecular synthons of cloxiquine (the electron density at BCP and RCP ( $\rho$ ), its Laplacian  $\Delta(\rho)$ , the potential electron energy density ( $V_{BCP}$ ), the kinetic electron energy density ( $G_{BCP}$ ) and the total electron energy density ( $H_{BCP}$ ) and energy of interaction ( $E_E$ ) calculated at the B3LYP/6-311++G(d,p) level of theory

COMPOUND	FORM	INTERACTION	R (X-H...Y)** [Å]	R(Y...H)*** [Å]	$\rho$ [a.u.]	$\Delta(\rho)$ [a.u.]	$\varepsilon$ [-]	$G_{BCP}$ [a.u.]	$V_{BCP}$ [a.u.]	$H_{BCP}$ [a.u.]	$E_E$ [kJ/mol]	STRENGTH
Cloxiquine	Form I RT [44] R=4.9%	O-H...N intermolecular	2.858	2.163	0.0172	0.0711	0.0455	0.0149	-0.0018	0.0131	-15.70	weak
		N(1)...N(1'')	3.373	-	0.0071	0.0203	1.0940	0.0045	-0.0038	0.0006	-5.01	weak
		C-H...O (interlayer)	3.475	2.809	0.0049	0.0170	0.1647	0.0036	-0.0029	0.0007	-3.77	weak
		Cl(5)...Cl(5')	3.814	-	0.0043	0.0140	0.0809	0.0027	-0.0018	0.0008	-2.37	weak
		C(6)...C(5')	3.814	-	0.0055	0.0150	0.1686	0.0031	-0.0025	0.0007	-3.23	weak
		C(10)...C(4')	3.451	-	0.0052	0.0143	0.8493	0.0029	-0.0023	0.0007	-2.97	weak
		C(8)...C(9')	3.487	-	0.0050	0.0134	0.4528	0.0028	-0.0022	0.0006	-2.82	weak
		N(1)-C(2')	3.455	-	0.0045	0.0134	0.4039	0.0028	-0.0022	0.0006	-2.85	weak
	Form I RT [44] opt*	O-H...N intermolecular	2.858	1.934	0.0302	0.0829	0.0369	0.0211	-0.0214	-0.0003	-28.09	weak
		C-H...O (interlayer)	3.475	2.782	0.0050	0.0176	0.1599	0.0037	-0.0030	0.0007	-3.92	weak
		Cl(5)...Cl(5')	3.814	-	0.0043	0.0140	0.0819	0.0027	-0.0018	0.0008	-2.39	weak
		C(6)...C(5')	3.814	-	0.0053	0.0149	0.2917	0.0031	-0.0024	0.0006	-3.21	weak
		C(10)...C(4')	3.451	-	0.0053	0.0145	0.8311	0.0029	-0.0023	0.0007	-2.99	weak
		C(8)...C(9')	3.487	-	0.0050	0.0135	0.5245	0.0028	-0.0021	0.0006	-2.81	weak
		N(1)-C(2')	3.455	-	0.0045	0.0135	0.4405	0.0028	-0.0022	0.0006	-2.89	weak
		Form I 90K [45] R=6.69%	O-H...N intermolecular	2.811	2.063	0.0230	0.0794	0.0453	0.0180	-0.0161	0.0019	-21.14
	C-H...O (interlayer)		3.392	2.791	0.0048	0.0180	0.1983	0.0037	-0.0029	0.0008	-3.82	weak
	Cl(5)...Cl(5')		3.745	-	0.0049	0.0163	0.0222	0.0031	-0.0022	0.0010	-2.82	weak
	C(6)...C(5')		3.395	-	0.0058	0.0165	0.2639	0.0034	-0.0027	0.0007	-3.58	weak
	C(10)...C(4')		3.388	-	0.0058	0.0158	0.7103	0.0032	-0.0025	0.0007	-3.30	weak
	C(8)...C(9')		3.407	-	0.0056	0.0155	0.6187	0.0032	-0.0025	0.0007	-3.21	weak
	N(1)-C(2')		3.388	-	0.0050	0.0149	0.1343	0.0031	-0.0025	0.0006	-3.23	weak
	Form II 90K [45] R=5.48% opt*		O-H...N intermolecular	2.833	2.131	0.0203	0.0681	0.0239	0.0152	-0.0133	0.0019	-17.44
		C-H...O intermolecular	2.999	2.471	0.0089	0.0406	0.6320	0.0082	-0.0063	0.0019	-8.32	weak
O-H...N intramolecular		2.742	2.181	0.0198	0.0774	0.9893	0.0171	-0.0149	0.0022	-19.61	weak	
Cl(5)...Cl(5')		3.763	-	0.0047	0.0157	0.0244	0.0030	-0.0021	0.0009	-2.70	weak	
C(6)...C(5')		3.763	-	0.0061	0.0173	0.3776	0.0036	-0.0028	0.0008	-3.73	weak	
C(10)...C(4')		3.405	-	0.0057	0.0158	0.9877	0.0032	-0.0025	0.0007	-3.28	weak	
C(8)...C(9')		3.373	-	0.0060	0.0165	0.8761	0.0034	-0.0026	0.0008	-3.43	weak	
N(1)-C(2')		3.413	-	0.0048	0.0145	1.1233	0.0030	-0.0023	0.0007	-3.06	weak	

\* partially optimized geometry, R – the reliability factor (R-factor)

\*\* R(X...Y) donor (X) – acceptor (Y) distance

\*\*\* R(Y...H) acceptor (Y) – proton (H) distance

**Table 4b** Topological parameters of  $\rho$  for the stacked supramolecular synthons of clioquinol (the electron density at BCP and RCP ( $\rho$ ), its Laplacian  $\Delta(\rho)$ , the potential electron energy density ( $V_{BCP}$ ), the kinetic electron energy density ( $G_{BCP}$ ) and the total electron energy density ( $H_{BCP}$ ) and energy of interaction ( $E_E$ ) calculated at the B3LYP/6-311++G(d,p) level of theory

COMPOUND	FORM	INTERACTION	R (X-H...Y)** [Å]	R(Y...H)*** [Å]	$\rho$ [a.u.]	$\Delta(\rho)$ [a.u.]	$\varepsilon$ [-]	$G_{BCP}$ [a.u.]	$V_{BCP}$ [a.u.]	$H_{BCP}$ [a.u.]	$E_E$ [kJ/mol]	STRENGTH
Clioquinol	Form Ia RT [43] R=10% opt*	O-H...N intermolecular	2.792	1.883	0.0342	0.0943	0.0392	0.0249	-0.0262	-0.0013	-34.42	medium
		O-H...C (interlayer)	3.347	2.661	0.0065	0.0226	0.0394	0.0048	-0.0039	0.0009	-5.16	weak
		Cl...Cl	4.139	-	0.0025	0.0072	0.8157	0.0014	-0.0010	0.0004	-1.27	weak
		I...I	4.141	-	0.0064	0.0169	0.1010	0.0035	-0.0028	0.0007	-3.63	weak
		I...C(7')	3.736	-	0.0069	0.0183	0.3565	0.0038	-0.0031	0.0007	-4.08	weak
		C(7)...C(4')	3.610	-	0.0044	0.0121	6.9864	0.0025	-0.0020	0.0005	-2.65	weak
		C(9)...C(3')	3.796	-	0.0046	0.0124	9.2978	0.0026	-0.0020	0.0006	-2.62	weak
	Form Ib RT [42] R=8.4% opt*	O-H...N intermolecular	2.850	1.942	0.0298	0.0900	0.0439	0.0212	-0.0212	0.0000	-27.83	weak
		O-H...C (interlayer)	3.359	2.645	0.0065	0.0226	0.1604	0.0048	-0.0039	0.0009	-5.12	weak
		Cl...Cl	4.160	-	0.0024	0.0069	0.0783	0.0013	-0.0009	0.0004	-1.21	weak
		I...I	3.710	-	0.0066	0.021	0.106	0.004	-0.0029	0.0012	-3.89	weak
		I...I	4.161	-	0.0062	0.0165	1.3390	0.0034	-0.0027	0.0007	-3.52	weak
		I...C(7')	3.732	-	0.0070	0.0181	0.3065	0.0038	-0.0031	0.0007	-4.09	weak
		C(7)...C(4')	3.609	-	0.0040	0.0114	2.4708	0.0023	-0.0018	0.0005	-2.40	weak
C(9)...C(3')	3.562	-	0.0047	0.0122	2.8017	0.0025	-0.0019	0.0006	-2.53	Weak		

\* partially optimized geometry, R – the reliability factor (R-factor)

\*\* R(X...Y) donor (X) – acceptor (Y) distance

\*\*\* R(Y...H) acceptor (Y) – proton (H) distance

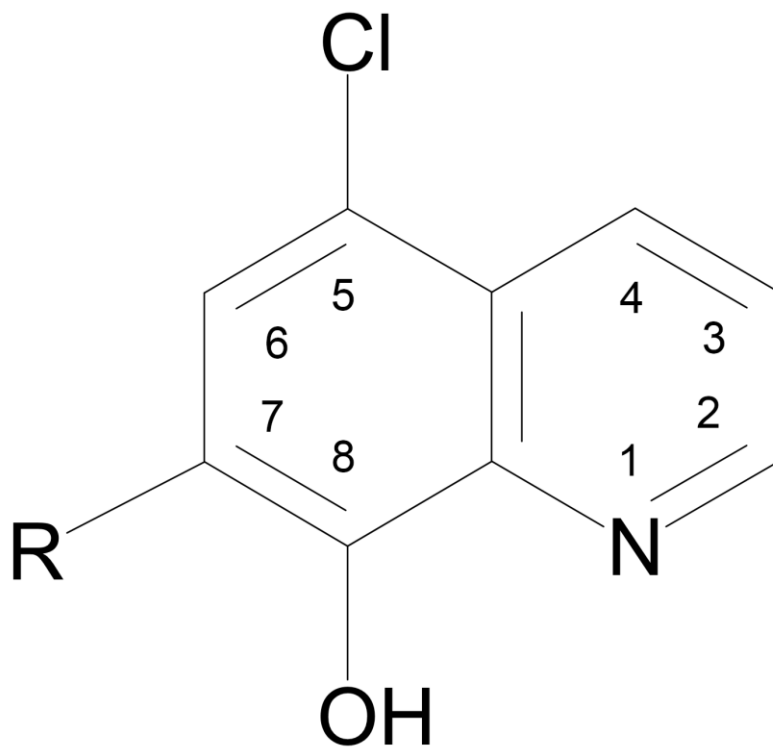
## Figure captions

- Fig. 1** The molecular structure of 8-quinolinol derivatives (R=I clioquinol, R=H cloxiquine)
- Fig. 2** The  $^{35}\text{Cl}$ -NQR spectra of clioquinol and cloxiquine at  $T = 77\text{ K}$
- Fig. 3** The  $^1\text{H}$ - $^{14}\text{N}$  solid effect double resonance spectra of clioquinol and cloxiquine at  $T = 295\text{ K}$ . The proton Larmor frequency is  $\nu_L = 100\text{ kHz}$
- Fig. 4** The  $^1\text{H}$ - $^{17}\text{O}$  double resonance spectra of cloxiquine at  $T = 213\text{ K}$  as measured by the Slusher and Hahn's technique (a) and by the two-frequency irradiation technique (b)
- Fig. 5** The correlation between the experimental and calculated NQR frequencies  
 (a) cloxiquine (form I at RT and 90K, form II),  
 (b) cloxiquine (form I), clioquinol (form Ia)
- Fig. 6** The orientation of EFG tensor axes at all quadrupolar sites:  
 cloxiquine (form I), first column,  
 cloxiquine (form II), second column,  
 clioquinol (form Ia), third column one of the axes is in each case perpendicular to the screen
- Fig. 7** Molecular graphs of 8-quinolinol derivatives:  
 cloxiquine (form I), supramolecular synthon,  
 cloxiquine (form II), supramolecular synthon,  
 clioquinol (form Ia), supramolecular synthon, dashed lines indicate the interactions, large circles correspond to attractors, small ones to critical points (red - RCP, green - BCP)
- Fig. 8** Relief map of the Laplacian of electron density in the  $\text{OH}\cdots\text{N}$  plane.  
 cloxiquine (form I), supramolecular synthon,  
 cloxiquine (form II), supramolecular synthon,  
 clioquinol (form Ia), supramolecular synthon

**Fig. 9** Molecular graphs of 8-quinolinol derivatives:  
 cloxiquine (form I), stacked supramolecular synthon,  
 cloxiquine (form II), stacked supramolecular synthon,  
 clioquinol (form Ia), stacked supramolecular synthon, dashed lines indicate the interactions, large circles correspond to attractors, small ones to critical points (green - BCP; RCP were omitted for clarity).

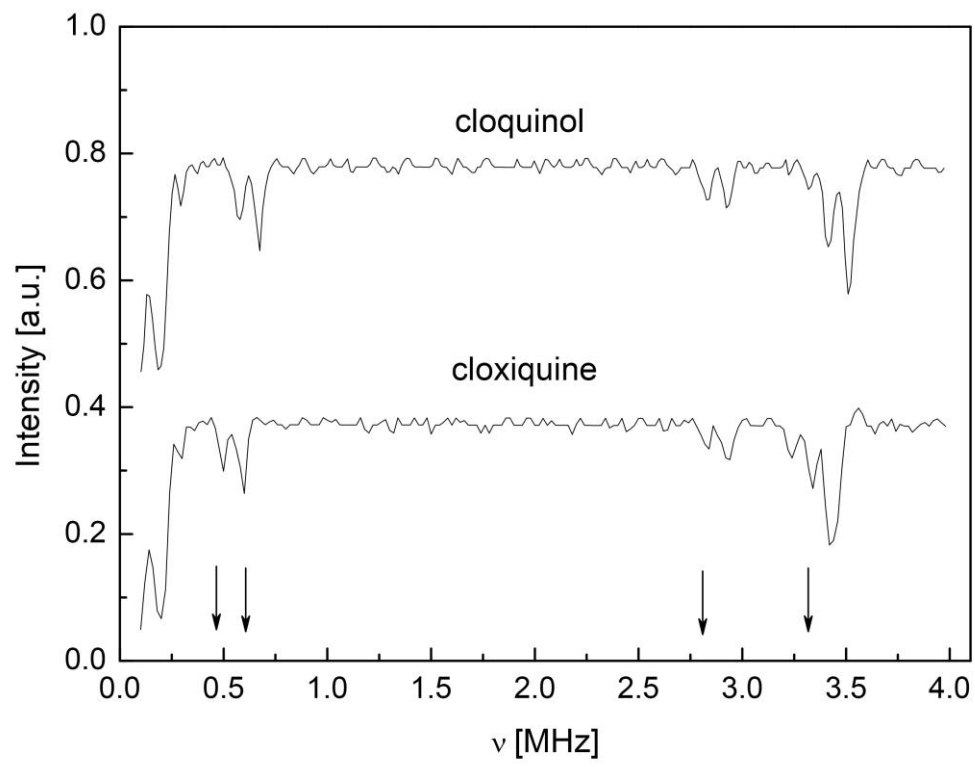
**Fig. 10** The relations between  
 (a)  $\rho$  (electron density at the critical point) and interaction energy (in  $\text{kJ mol}^{-1}$ ),  
 (b)  $\Delta\rho$  (Laplacian of electron density at the critical point) and interaction energy (in  $\text{kJ mol}^{-1}$ ),  
 (c) energy of hydrogen bond interactions  $E_E$  (in  $\text{kJ mol}^{-1}$ ) calculated using the Espinosa method assuming dimer and stacked dimers (solid line linear fit, correlation coefficient 0.999, standard deviation  $0.02 \text{ kJ mol}^{-1}$  and slope  $1.004 \text{ kJ mol}^{-1}$ )

**Fig. 11** The relations between  
 (a) H...Y distance ( $R_{H...Y}$ ) and hydrogen bond energy (in  $\text{kJ mol}^{-1}$ ); solid line fit with a parabola, correlation coefficient 0.989, standard deviation  $11.9 \text{ kJ mol}^{-1}$   
 (b) H...Y distance ( $R_{H...Y}$ ) and  $\rho$  (electron density at the critical point); solid line fit with an exponential function, correlation coefficient 0.998, standard deviation  $2.4 \cdot 10^{-6}$  a.u.  
 (c) H...Y distance ( $R_{H...Y}$ ) and  $\Delta\rho$  (Laplacian of electron density at the critical point); solid line fit with a linear function correlation coefficient 0.988, standard deviation  $1.2 \cdot 10^{-4}$  a.u. slope  $-0.085$  a.u.



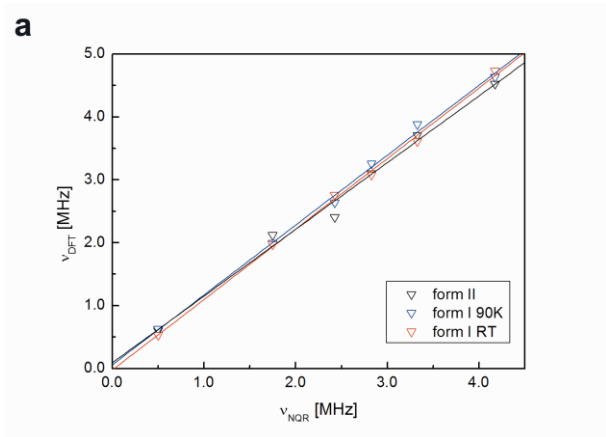




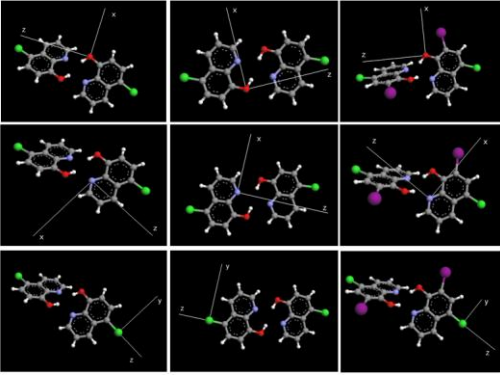


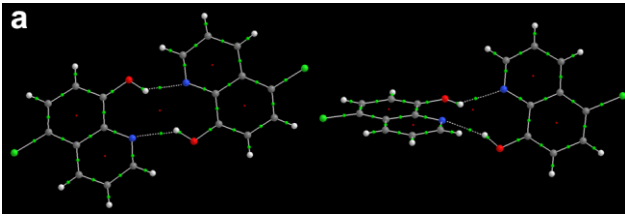


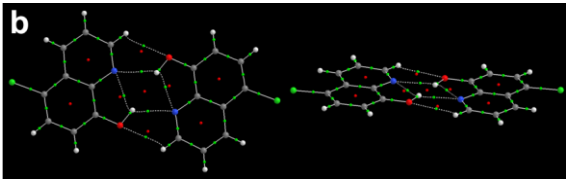


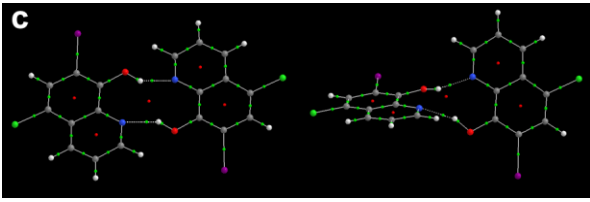


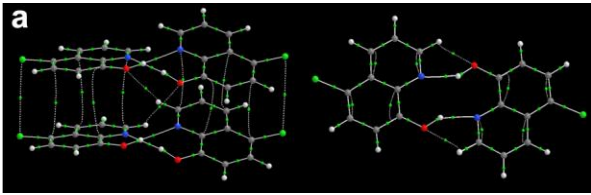


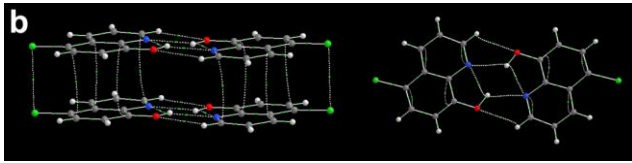


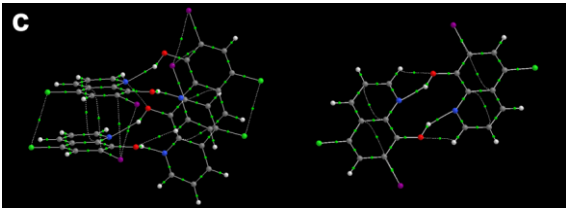


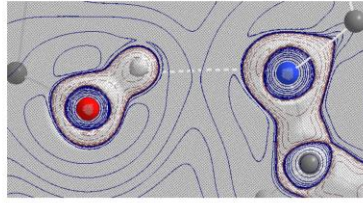
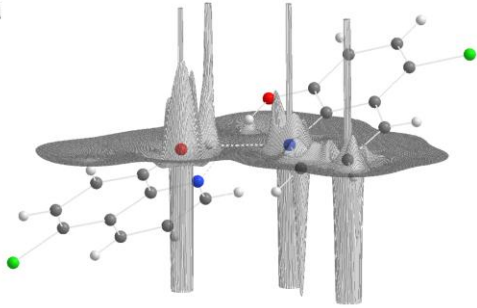
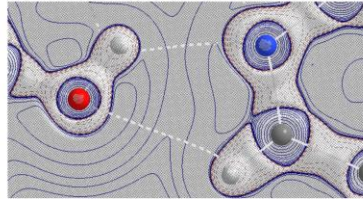
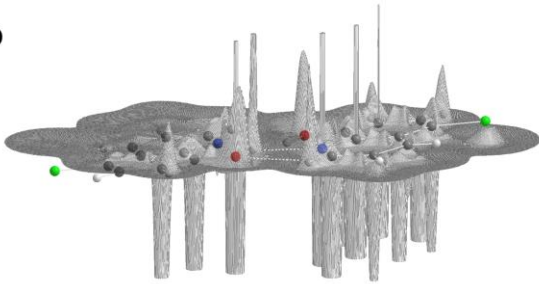










**a****b**

**C**